Engineering butylglyceryl-modified polysaccharides towards nanomedicines for brain drug delivery

Mohammad F. Bostanudin[a,b], Aikaterini Lalatsa[b], Dariusz C. Górecki[b], Eugen Barbu[b,*]

[a]College of Pharmacy, Al Ain University, Abu Dhabi 112612, UAE
[b]School of Pharmacy and Biomedical Sciences, University of Portsmouth, St Michael's Building, White Swan Road, PO1 2DT, United Kingdom

Abstract

Colloidal systems prepared from carbohydrates are subject of intense research due to their potential to enhance drug permeability through biological membranes, however their characteristics and performance are never compared directly. Here we report the results of a comparative investigation of a series of butylglyceryl-modified polysaccharides (chitosan, guar gum, and pullulan) that were formulated into nanoparticles and loaded with a range of model actives (Doxorubicin, Rhodamine B, Angiotensin II). Butylglyceryl-modified guar gum and corresponding pullulan nanocarriers were more stable at physiological pH compared to those obtained from modified chitosan, and studies of the in-vitro interactions with mouse brain endothelial cells (bEnd3) indicated an increased biological membrane permeability and lack of toxicity at application-relevant concentrations. No significant haemolytic effect was observed, and confocal microscopy and flow cytometry studies confirmed the efficient cellular uptake and cytoplasmic localisation of NPs. Most promising characteristics for brain drug delivery applications were demonstrated by butylglyceryl pullulan nanocarriers.

Keywords: nanoparticles; pullulan; guar gum; chitosan; polysaccharides; drug delivery; brain.

1. Introduction

A significant number of brain disorders are considered responsible for the rising morbidity and mortality observed in both developed and developing countries (Raggi & Leonardi, 2019), but real progress in the treatment of many neurological disorders has been long hindered by the inability of most drugs to enter the brain – despite recent technological advances, the blood-brain barrier (BBB) continues to represent a major challenge (Aikaterini

Lalatsa & Barbu, 2016). In concerted efforts to enhance drug concentration in the brain, many strategies have been considered, however it has been found that the benefits registered with several invasive methods come at the rather high cost of harmful side effects (Aikaterini Lalatsa, Schatzlein, & Uchegbu, 2014). Current research tends therefore to concentrate on non-invasive strategies, with the use of colloidal drug carriers as a most promising approach for systemic brain delivery (Godfrey et al., 2018; Lu et al., 2014).

Among the carbohydrates investigated, of particular interest are polysaccharides: they are highly stable, non-toxic, biodegradable, possess hydrophilic moieties that mediate non-covalent interactions with biological tissues (Hervé, Ghinea, & Scherrmann, 2008), and can be converted into amphiphilic materials that self-assemble into colloidal carriers (Bostanudin, Arafat, Sarfraz, Górecki, & Barbu, 2019; A. Lalatsa et al., 2015; Toman et al., 2015). Due to its low cost, widespread availability and ease of chemical modification, chitosan (CS) has been one of the most intensively studied polysaccharides for brain drug delivery applications, demonstrating indeed very promising results (A. Lalatsa et al., 2015; Lien et al., 2012; Toman et al., 2015). Rationalised by the ability of short chain alkylglycerols to enhance drug access into the brain *in vivo* when administered intracarotidally (Erdlenbruch et al., 2003), dextran and chitosan have been previously modified with alkylglycerols and formulated into nanoparticles, which were shown to be taken up by endothelial brain cells and to increase drug permeability *in vitro* and *in vivo* (Boussahel et al., 2017; Ibegbu, Boussahel, Cragg, Tsibouklis, & Barbu, 2017; Lien et al., 2012; Molnár, Barbu, Lien, Górecki, & Tsibouklis, 2010; Toman et al., 2015). In contrast to chitosan, polysaccharides of similar generic features but lacking a ionisable amino group that can negatively impact on the nanomedicines' colloidal stability, such as pullulan (PUL) and guar gum (GG), have been less investigated for their potential in similar drug delivery applications (Singh, Kaur, Rana, & Kennedy, 2017). Also, to our knowledge, no comparative investigations into the characteristics and *in vitro* performance (such as drug loading, brain cells uptake and permeability) of different polysaccharides have been reported.

Investigating the hypothesis that nanomedicines based on amphiphilic pullulan and guar gum can provide improved characteristics relevant to brain drug delivery applications compared to similarly-modified chitosan-based materials, we describe here the preparation and characterisation of colloidal formulations obtained from novel butylglyceryl-modified PUL and GG and loaded with a range of model actives (Doxorubicin, Rhodamine B, Angiotensin II). Results of *in vitro* investigations comparing the interactions of these nanocarriers with mouse brain endothelial cells (bEnd3) in terms of cytotoxicity, cellular uptake and BBB model

membrane permeability, relative to butylglyceryl-modified CS nanoparticles, are also presented.

2. Materials and methods

2.1. Materials

Low molecular weight (MW) chitosan (MW 50–190 kDa; 75-85% deacetylation; cat. no. 448869; batch no. MKBD0020), pullulan (MW 100 kDa; cat. no. 91335; batch no. BCBK3803V), guar gum (MW 220 kDa; cat. no. G4129; batch no. 041M0058V), dimethylformamide (DMF; anhydrous, 99.8%), dimethyl sulfoxide (DMSO; anhydrous, ≥ 99.9%), nbutylglycidyl ether (BGE; reagent grade 95%), potassium *tert*-butoxide (t-BuOK; reagent grade > 97%), phthalic anhydride (reagent grade ≥ 99.9%), sodium tripolyphosphate (TPP), sodium hydroxide (NaOH), Span 80, glycerol (reagent grade ≥ 99.5%), glutaraldehyde (25% in H_2O; cat. no. G6257), Rhodamine B base (Dye content 97%), Angiotensin II human (HPLC grade ≥ 93%), Triton X-100, Hydrocortisone (HPLC grade ≥ 98%), Adenosine 3',5'-Cyclic Monophosphate (HPLC grade ≥ 98.5%) and Fluorescein Isothiocyanate (FITC) labelled dextran (MW 500 kDa) were sourced from Sigma Aldrich (Gillingham, UK).

Hydrazine monohydrate, acetic acid, dimethylsulfoxide (DMSO, analytical grade), and dichloromethane (DCM) were purchased from Fisher Scientific (Loughborough, UK). Doxorubicin was obtained from Carbosynth (Compton, UK). Texas Red-X succinimidyl ester (mixed isomers), Texas Red-X dichlorotriazine, Dulbecco's Modified Eagle Medium (DMEM) media, NucGreen Dead 488 and TrypLE Express were sourced from Life Technologies Ltd. (Paisley, UK). Phosphate Buffered Saline (PBS) was purchased from Gibco (Paisley, UK). Forskolin and RO-20-1724 were obtained from Enzo Life Sciences (Exeter, UK).

2.2. Synthesis and characterisation of butylglyceryl-modified polysaccharides

The synthesis was adapted from methods described in the literature (Bostanudin et al., 2019; Molnár et al., 2010), with some modifications. Briefly, an alkaline solution of polysaccharide (either 2.78 mmol GG, 3.05 mmol PUL or 4.39 mmol phthaloylated CS, dissolved in either water, DMSO, or DMF, respectively) was reacted with *n*-butylglycidyl ether in different ratios (3–114 mmol, *Figure 1)*. The reaction mixture was left stirring overnight then purified by washing (x3) with DCM and/or dialysis (MWCO 3.5 kDa, Medicell Ltd, London, UK) against deionised water (10 L; 9 changes over 72 h) prior to lyophilisation. All

materials were characterised by ^{1}H-NMR spectroscopy using a JEOL Eclipse 400+ instrument (JEOL, Welwyn Garden City, UK; 400 MHz) and the degree of substitution (DS) was calculated from the ^{1}H-NMR spectra. FT-IR spectra were recorded on a Nexus Euro infrared spectrometer (Thermo Fisher Scientific, Hemel Hempstead, UK) and Gel permeation chromatography (GPC) was performed using a Waters Alliance GPC 2000 system (Waters Corporation, Milford, MA, USA) (details in the *Supplementary Materials*)

2.3. Formulation of butylglyceryl-modified guar gum nanoparticles

Span 80 (0.4 g) solution in DCM (3.33 mL) was added to a butylglyceryl-modified GG; GG-OX4 solution (10 mL) of specific concentration (0.5–2% w/v; different DS) under stirring. Glycerol (1 mL) was added, followed by glutaraldehyde (1 mL; 3% v/v) under stirring and was left stirring overnight prior to ultracentrifugation (x3 ultracentrifuge; Beckman Coulter, High Wycombe, UK; 70.1 Ti rotor; 164,391 g; 30 min); the pellet was washed three times with deionised water and freeze-dried, affording nanoparticles as white powder (55–65% yield).

2.4. Formulation of butylglyceryl-modified pullulan nanoparticles

Butylglyceryl-modified PUL solution; PUL-OX4 in DMSO (2 mL) at varying concentrations (1–10 mg/mL; different DS) was added to ultrapure water (8 mL) under stirring. The nanoparticles were dialysed (MWCO 12-14 kDa, Medicell Ltd, London, UK) against deionised water (10 L; 9 changes over 72 h) and lyophilised, affording nanoparticles as beige powder (yields 76–83%).

2.5. Formulation of butylglyceryl-modified chitosan nanoparticles

Sodium tripolyphosphate (2 mL) aq. solution at varying concentrations (0.1–0.3 mg/mL) was introduced dropwise (1 mL/min) under stirring to butylglyceryl-modified chitosan solution; CS-OX4 (1.07–2.5 mg/mL; various DS) in aq. acetic acid (1% v/v, 6 mL). The nanoparticles were ultracentrifuged (164,391 g; 30 min), washed (x3) with deionised water, and lyophilised, affording nanoparticles as beige powder (yields 16–45%).

2.6. Morphological characterisation

The nanoparticles diameter was determined by dynamic light scattering (DLS) using a Malvern ZetasizerNano ZS instrument equipped with a 633 nm He-Ne laser (173° scattering angle) (Malvern Instruments Ltd., Worcestershire, UK), calibrated by 100–400 nm polystyrene

latex standard beads and DTS 1050 latex beads (Malvern Instruments Ltd). Samples were analysed (x3) at 25 °C and the results were expressed as Z-average mean and polydispersity index (PDI). Electrophoretic mobility measurements were conducted using the same instrument to determine the ZP. Investigation on nanoparticles stability at varying pH values (3–8.5) was performed employing a Multi-Purpose Titrator-2 instrument (Malvern Instruments Ltd.). The nanoparticles were redispersed (0.5 mg/mL) in an ultrapure water and the pH was adjusted with NaOH solution (0.005 M), and HCl (0.05 M); the diameter and ZP were measured at 0.5 pH increments. Complementary size determination was conducted using a Nanoparticle Tracking Analysis (NTA) LM-14 instrument (Malvern Instruments Ltd.) equipped with a 532 nm green laser at 25 °C.

Scanning Electron Microscopy (SEM) was performed by depositing aqueous nanoparticles dispersion (5 mg/mL) onto a metallic stub prior to coating with Au/Pd under argon using a Q150RES sputter coater (Quorum Technologies Ltd., Ashford, UK), and imaged using a JEOL-JSM-6060LV SEM Microscope (JEOL). For Transmission Electron Microscopy (TEM), aq. dispersion (5 mg/mL) was placed onto the TEM copper grid surface (3.0 mm, 200 mesh, coated with Formvar film), stained with 2% (w/v) uranyl acetate staining solution and imaged with a JEOL JEM 2100 TEM Microscope (JEOL).

2.7. Model actives loading and release studies

A solution of either Rhodamine B (0.5 mL; 0.037 mg/mL in DMSO), Doxorubicin (0.5 mL; 0.4 mg/mL in DMSO) and Angiotensin II (1 mL; 0.1 mg/mL in deionised water) were mixed with polymer solution during nanoparticles preparation *via* various techniques (section 2.3−2.5). The nanoparticles were ultracentrifuged (164,391 g; 30 min); the pellets were lyophilised and weighed; the supernatant was measured for the unbound model actives amount by UV/Vis spectroscopy measurements employing a Lambda 650 Ultra Violet/Visible Spectrometer (Perkin Elmer, Buckinghamshire, UK; measuring at 544 nm for Rhodamine B; 486 nm for Doxorubicin). For Angiotensin II detection, HPLC analysis was performed using an Agilent 1100 series HPLC system (Agilent Technologies, Waldbron, Germany; C18 reversed phase column; acetonitrile/trifluoroacetic acid (TFA) 99.9:0.1 v/v, linear gradient 10−60% (0.7 ml/min); retention time = 8.32 min; lower detection limit = 25 ng/mL. The drug loading was calculated using Equation (2):

$$DL\ (\%) = \frac{weight\ of\ drug}{weight\ of\ nanoparticles}\ x\ 100 \qquad (2)$$

For the release studies, nanoparticles were re-dispersed (1.5 mg/mL) in PBS (pH 7.4; saline 0.9%), aliquots (1.5 mL) were taken and distributed into Eppendorf tubes, which were then placed in a thermostatic (37 °C) shaking water bath. At varying time points, an aliquot (700 µL) was individually removed from the supernatant and analysed using either HPLC or UV/Vis.

2.8. Nanoparticles fluorescent labelling

A Texas Red-X dichlorotriazine solution in DMSO (0.5 mL; 2 mg/mL) was added to either GG-OX4 in 0.1 M sodium bicarbonate buffer (10 mL; 10 mg/mL) or PUL-OX4 solution in DMSO/0.1 M sodium bicarbonate buffer (70:30 v/v; 10 mL; 10 mg/mL) under stirring. CS-OX4 labelling was performed employing Texas Red-X succinimidyl mixed ester in DMSO (0.5 mL; 2 mg/mL), where it was added to the polymer dispersion in 0.1 M sodium bicarbonate buffer (10 mL; 10 mg/mL) under stirring; maintained for 1 h. Labelled GG-OX4 and PUL-OX4 was precipitated with DCM, centrifuged (2,880 g; 30 min) using a Jouan B4i (Thermo Fisher Scientific), purified by either washing (x3) with DMSO for labelled CS-OX4 or dialysis (MWCO 12-14 kDa) against deionised water (10 L; 3 exchanges over 24 h) for labelled GG-OX4 and PUL-OX4 and then lyophilised, affording Texas Red-labelled polymer; GG-OX4 as a purple and fluffy cotton-like material (yields 78– 81%), PUL-OX4 and CS-OX4 as a purple powder (yields 71–73% and 71–75% respectively). The degree of labelling was analysed by UV/Vis spectroscopy (measuring at 589 nm) and calculated using Equation (3):

$$Degree\ of\ labelling\ (\%) = \frac{weight\ of\ Texas\ Red}{weight\ of\ nanoparticles} \times 100 \qquad (3)$$

2.9. Cell culture

Mouse brain endothelial (bEnd3) cells were obtained from the European Collection of Cell Cultures (ECACC). The cells (passage no. 37–45) were cultured in a modified DMEM media, enriched with supplements (*Table S1, Supplementary Materials*). The cells were grown at 37ºC with 5% CO_2 under humidified atmosphere in an incubator. Trypsinisation was performed with TrypLE Express and flasks were equilibrated at 37ºC for 10–15 min. The cell suspension was harvested (115 g; 5 min) using a Beoco C28A (Wolf Laboratories, Pocklington, UK) for further use.

2.10. Cytotoxicity assays

Nanoparticles (50 µL; dispersed in modified DMEM at concentrations 1–10 mg/mL) were incubated with confluent bEnd3 cells (seeding 4.0 x 10^4). Sterile PBS and Triton-X (0.1% v/v) were used as negative and positive controls respectively. After 24 h incubation, media was replaced with MTT solution (100 µL, 1 mg/mL) and incubated (37^{o}C) for another 1 h prior to be replaced by DMSO (100 µL) and analysed using a POLARstar OPTIMA (BMG Labtech, Aylesbury, Bucks, UK; measuring at 570 nm).

2.11. Confocal microscopy analysis

Nanoparticle suspension in modified DMEM (2 mL; 0.5 mg/mL) were incubated with confluent bEnd3 cells (seeding 4.0 x 10^4) for 3 h; cells without nanoparticles were used as a control. The cells were washed (x3) with PBS, fixed in paraformaldehyde (4% w/v; 4^{o}C) and permeabilised with Tween 20 (0.1% v/v) prior to 15 min incubation with NucGreen Dead 488 before visualisation using a confocal microscope (LSM 510 META, ZEISS, Carl Zeiss, Oberkochen, Germany; 488 nm for NucGreen and 543 nm for Texas Red).

2.12. Flow cytometry analysis

Doxorubicin-loaded nanoparticles (2 mL; 0.5 mg/mL in modified DMEM) were incubated with confluent bEnd3 cells (seeding 4.0 x 10^4) for 3 h. The cells were harvested (115 g; 5 min) and redispersed in PBS (400 µL) for analysis. Cells treated with propidium iodide (1% v/v; without nanoparticles) were used as a control. Flow cytometry was performed on a four-colour multi parameter BD FACSCalibur system (BD Biosciences, Oxford, UK) equipped with a 488 nm argon gas laser and a 635 nm red-diode laser; Doxorubicin emission fluorescence was measured using a 530/30 nm filter.

2.13. Fluorescent marker translocation across bEnd3 cell monolayers studies

bEnd3 cells were seeded (4 x 10^4 cells) in a Transwell-type BBB model comprising of a sterile 24-well plate Millipore Millicell; incubated at 37^{o}C until confluent. A specific cocktail (consisting of cAMP (250 µM), RO-20-1724 (20 µM), Forskolin (50 µM) and hydrocortisone (550 µM)) was applied and incubation continued for another 24 h. Nanoparticles (2 mg/mL) and FITC-dextran (100 µg/mL) dispersed in media were simultaneously applied to each well and the FITC-dextran concentration in the basolateral compartment was then monitored; samples (100 µL) were collected every 30 min (for 3 h) for analysis using a POLARstar OPTIMA fluorescence plate reader (BMG Labtech) (485 nm/520 nm excitation/emission

wavelengths). The apparent permeability coefficient (Papp) was calculated based on Equation (4):

$$Papp\ (cm.s^{-1}) = \frac{dQ}{dt} \times \frac{V_R}{A \times Co \times 60} \quad (4)$$

where;

dQ/dt	FITC-dextran flux transported across the membrane (µg/sec)
V_R	basolateral volume (600 µL)
A	filter insert surface area (0.33 cm^2)
Co	FITC-dextran initial mass concentration at the apical side (100 µg/mL)
60	conversion factor (min to s)

2.14. Haemolysis studies

Blood was obtained from a male Wistar rat (450 g), after CO_2 asphyxiation, by collection from the heart using a 21G needle into a BD Vacutainer tube (lithium heparin) and kept on ice. The red blood cells (RBC) were separated by centrifugation (Heraeus Multifuge 3SR Plus; 2000 g; 10 min; 4ºC); the plasma fraction was removed before washing the RBC with PBS (x3) and centrifuged (2,000 g; 10 min), before dilution with PBS (4% w/v) to yield a cell suspension. PBS and Triton-X (1% v/v) were used as negative and positive controls respectively. NPs suspensions were added (10 µL) to RBC cell suspension (190 µL) and then incubated (37 ºC) for 1 h prior to centrifugation (1200 g; 10 min; 4ºC); the supernatant (150 µL) absorbance was measured at 570 nm using a Multiskan GO microplate reader (Thermo Fisher Scientific). Haemolysis percentage was calculated using Equation (5):

$$Haemolysis\ (\%) = \frac{Sample_{Absorbance} - negative\ control_{Absorbance}}{Positive\ control_{Absorbance} - negative\ control_{Absorbance}} \times 100 \quad (5)$$

2.15. Data statistical analysis

Statistical analysis was performed using SPSS Statistics v.22 software (SPSS Inc., Chicago, IL, USA, 2013). Results were expressed as mean ± standard deviation (SD) values; significance was tested using analysis of variance (ANOVA), p values were set at 0.05, unless stated otherwise.

3. Results and discussion

Butylglyceryl-modified polysaccharides were synthesised *via* a nucleophilic substitution reaction using *n*-butylglycidyl ether (*Figure 1*) as follow: GG-OX4 synthesis was achieved under strong alkaline conditions (aq. NaOH, pH 14); PUL-OX4 preparation was performed in DMSO with t-BuOK as a base; and CS-OX4 has been prepared by protecting the free amino groups with phthaloyl moieties, followed by butylglyceryl pendant chain attachment to the available polysaccharidic hydroxyl groups and phtahloyl groups removal using hydrazine (Molnár et al., 2010). Their structures were confirmed by FT-IR and ^{1}H-NMR spectroscopy, with molecular weight between 100kDa and 300kDa as measured by GPC (*Figures S1–S3, Supplementary Materials).*

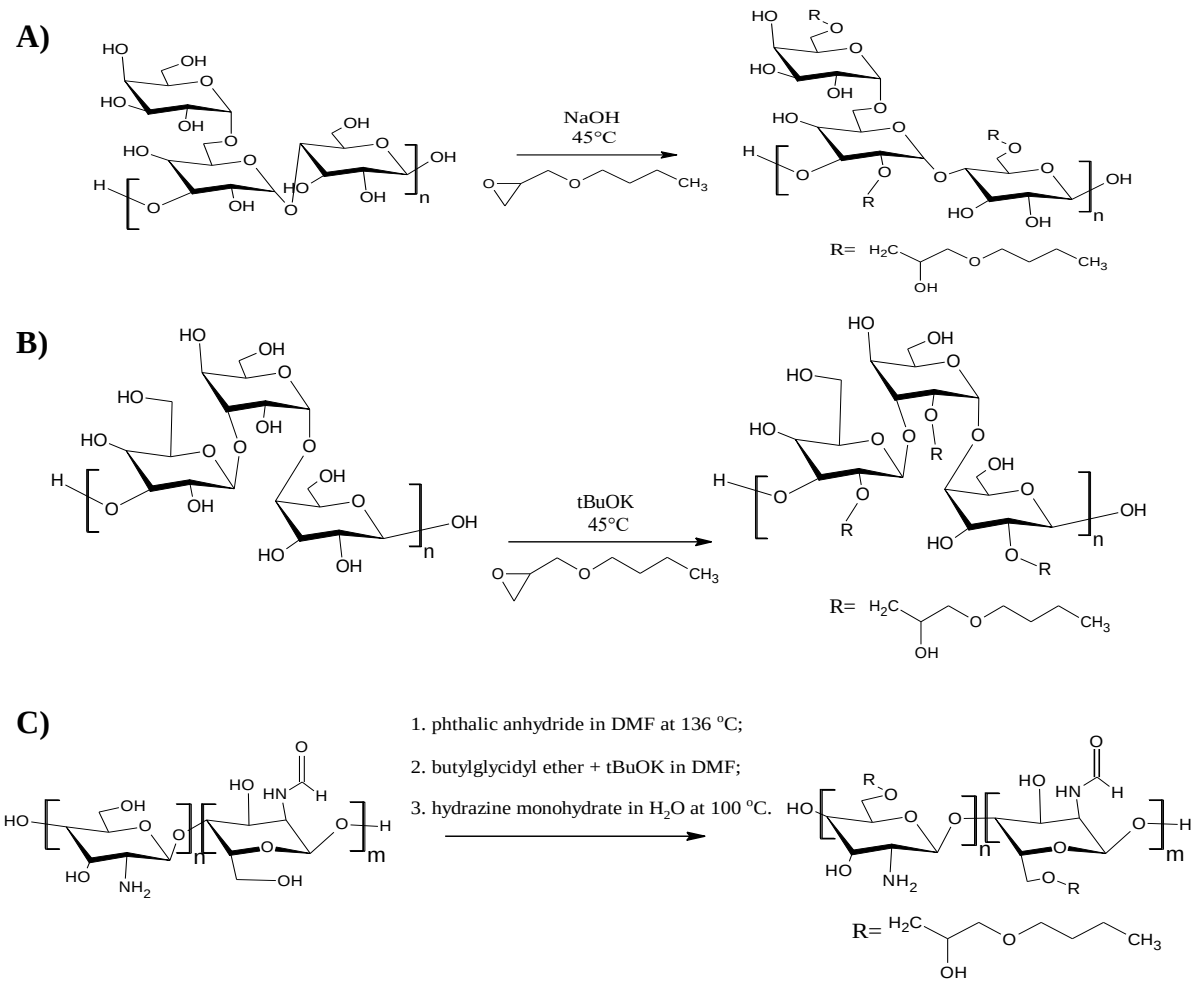

Figure 1. Schematic synthesis of: A) GG-OX4, B) PUL-OX4, and C) CS-OX4.

GG-OX4, CS-OX4, and PUL-OX4 derivatives with different degree of substitution (DS) have been formulated into nanoparticles with characteristics summarised in Table 1. The

size of nanoparticles was found to increase very slightly with concentration, possibly an effect due to a corresponding increase in viscosity (Chen, Mohanraj, Wang, & Benson, 2007). Reverse emulsification was employed to formulate GG-OX4 nanoparticles using glutaraldehyde as a cross-linker. Results *(Table 1)* indicate that GG-OX4 with lower DS values (DS 3.6, 12.6 and 33.9%) produced nanoparticles (yields 57–67%) with size in the range of 145–200 nm, with good PDI (ca. 0.2) and negative ZP values (-22 to -33 mV). PUL-OX4 nanoparticles with different DS and concentrations were prepared by nanoprecipitation, when nanoparticles around 120–180 nm, with good PDI (ca. 0.2) and negative ZP values (-23 to -32 mV) were obtained. CS-OX4 nanoparticles were prepared by ionotropic gelation with TPP, and results suggest that the yields increased with the TPP concentration (optimum 0.2 mg/mL), yielding nanoparticles (yields ~33%) with size around 145 (measured by DLS and NTA), monodispersed (PDI=0.32) and positive ZP value (34.1 mV). The ZP was found to decrease with an increase in the TPP concentration, likely because of the negatively charged TPP.

Table 1. Characteristics of nanoparticles at varying concentrations and DS (n=3; ±SD).

Material	DS (%)	Polymer conc. (% w/v)	TPP conc. (mg/mL)	Diameter NTA (nm)	Diameter DLS (nm)	Polydispersity Index	Zeta Potential (mV)	Yield (% w)
GG-OX4	3.6	0.5	N/A	145 ± 12	169 ± 9	0.22 ± 0.02	-32.7 ± 5.2	67 ± 5
		1.0		157 ± 15	17 ± 7	0.19 ± 0.02	-28.8 ± 2.9	57 ±15
		2.0		172 ± 16	200 ± 11	0.29 ± 0.03	-27.1 ± 7.0	58 ± 13
	12.6	0.5		166 ± 11	166 ± 3	0.21 ± 0.09	-29.9 ± 4.6	60 ± 10
		1.0		167 ± 13	170 ± 5	0.18 ± 0.06	-23.8 ± 1.9	58 ± 8
		2.0		178 ± 9	186 ± 8	0.15 ± 0.11	-22.1 ± 3.0	62 ± 9
	33.9	0.5		167 ± 11	167 ± 4	0.24 ± 0.04	-32.4 ± 6.2	61 ± 10
		1.0		176 ± 11	177.0 ± 11	0.20 ± 0.09	-25.5 ± 2.9	66 ± 11
		2.0		189 ± 17	192 ± 6	0.17 ± 0.10	-30.1 ± 5.7	59 ± 9
PUL-OX4	47.0	1	N/A	139 ± 22	143 ± 12	0.20 ± 0.10	-29.2 ± 2.8	79 ± 5
		5		157 ± 20	155 ± 6	0.18 ± 0.07	-27.9 ± 1.7	80 ± 4
		10		177 ± 17	182 ± 8	0.14 ± 0.06	-29.9 ± 1.4	81 ± 4
	58.5	1		133 ± 16	136 ± 15	0.21 ± 0.08	-23.4 ± 1.9	76 ± 5
		5		141 ± 12	145 ± 9	0.19 ± 0.11	-28.2 ± 3.3	77 ± 7
		10		158 ± 18	163 ± 8	0.17 ± 0.02	-30.1 ± 5.2	76 ± 9
	77.3	1		124 ± 23	125 ± 13	0.18 ± 0.12	-29.0 ± 4.3	82 ± 7
		5		132 ± 19	142± 12	0.17 ± 0.09	-31.9 ± 5.1	83 ± 5
		10		141 ± 20	178 ± 9	0.21 ± 0.05	-29.8 ± 2.9	79 ± 9
CS-OX4	14.1	1.07	0.10	153 ± 32	172 ± 18	0.33 ± 0.10	40.2 ± 1.7	16 ± 4
	14.1		0.15	156 ± 38	153 ± 17	0.36 ± 0.09	38.2 ± 1.4	22 ± 4
	14.1		0.20	146 ± 34	146 ± 26	0.32 ± 0.07	34.1 ± 2.1	33 ± 4
	30.5			157 ± 28	148 ± 24	0.25 ± 0.02	33.8 ± 3.0	31 ± 4
	51.1			167 ± 32	156 ± 11	0.25 ± 0.01	31.9 ± 0.6	27 ± 3
	14.1		0.30	289 ± 23	241 ± 14	0.31 ± 0.03	31.1 ± 1.4	45 ± 7
	14.1	1.50	0.20	167 ± 31	167 ± 16	0.31 ± 0.07	32.4 ± 2.0	28 ± 3
	14.1	2.00	0.20	218 ± 17	171 ± 15	0.35 ± 0.05	33.7 ± 1.8	34 ± 3
	14.1	2.50	0.20	324 ± 25	192 ± 17	0.27± 0.12	36.3 ± 1.3	36 ± 4

The stability of polysaccharide nanoparticulate suspensions was studied at various pH values in the range 3 to 8.5, with the main results being summarised in *Figure 2*. PUL-OX4 nanoparticles demonstrated better stability compared to the other materials under investigation, showing only a slight increase in size; the diameter remained always below 200 nm, as the modified pullulan was unaffected by pH changes due to the absence of ionisable groups (Barbosa, Abdelsadig, Conway, & Merchant, 2019). For GG-OX4 nanoparticles, an increase in size and a decrease in zeta potential were noticed at pH ≤4, where acidic conditions likely catalysed additional intermolecular cross-linking between the existing hemiacetals and the hydroxyl groups present on neighbouring macromolecules, leading eventually to agglomeration (Hongbo, Yanping, Wen, & Siqing, 2016; Pal, Paulson, & Rousseau, 2009). Freshly formulated CS-OX4 nanoparticles were cationic (with zeta potential around + 30 mV), and showed a stable diameter in acidic conditions (ca. 140 nm). However, as the pH increased above the pKa value of chitosan (ca. 6.3 (Wang et al., 2006)), a significant augmentation in diameter accompanied by a noticeable loss of stability (resulting from the deprotonation of the amine groups in chitosan around the isoelectric point) were observed.

A)

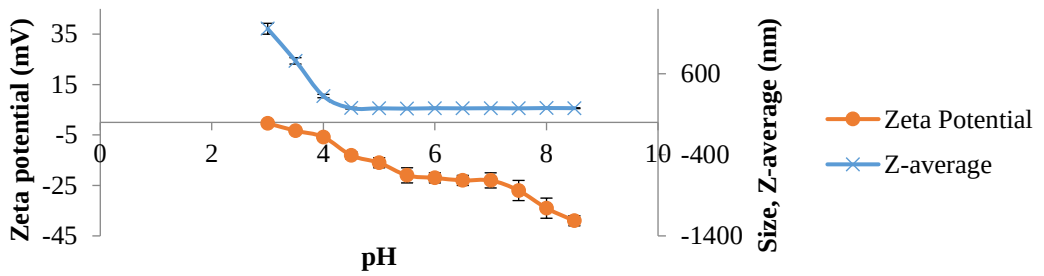

B)

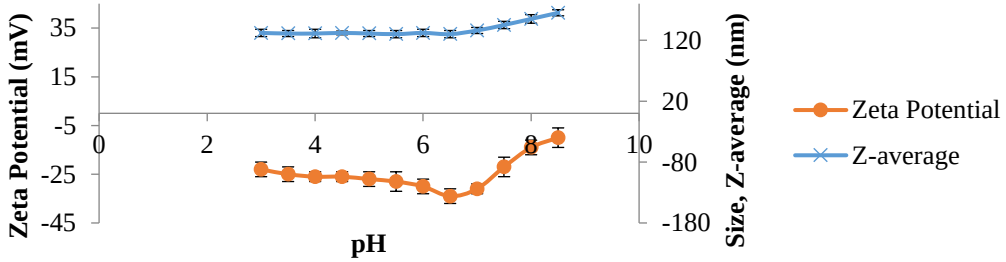

C)

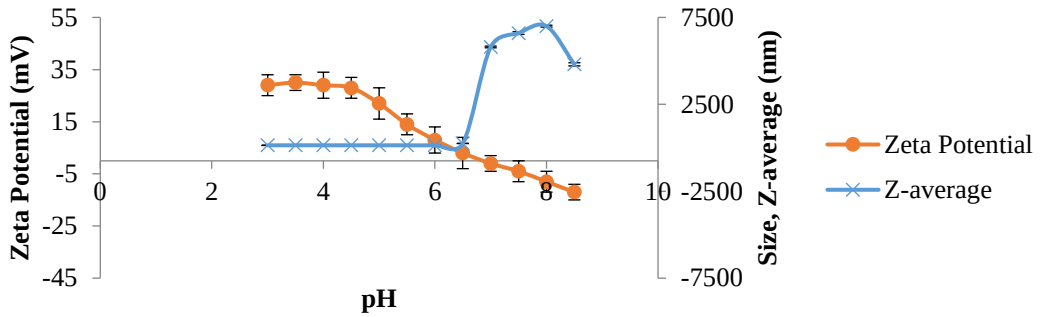

Figure 2. The influence of pH on the size and zeta potential of: A) GG-OX4, B) PUL-OX4, and C) CS-OX4 nanoparticles (1 mg/mL) (n=3, ±SD).

The nanoparticle morphology is exemplified in *Figure 3*. GG-OX4 and CS-OX4 nanoparticles were found to have the tendency to agglomerate during the purification and lyophilisation stages; the larger residual fragments visible in their SEM images (ribbon-like in Figure 3a, and fibre-like in Figure 3C) are attributed to the cross-linking reactions (with glutaraldehyde and sodium tripolyphosphate, respectively) employed during the formulation of these types of nanoparticles and drying during SEM sample preparation. PUL-OX4 nanoparticles showed a close to spherical morphology, in accordance with literature (Jung, Jeong, Kim, & Kim, 2004). SEM image indicated the CS-OX4 NPs were packed together after centrifugation and lyophilisation, which also affected their morphology. TEM images for PUL-OX4 and CS-OX4 NPs confirmed their spherical-like shape.

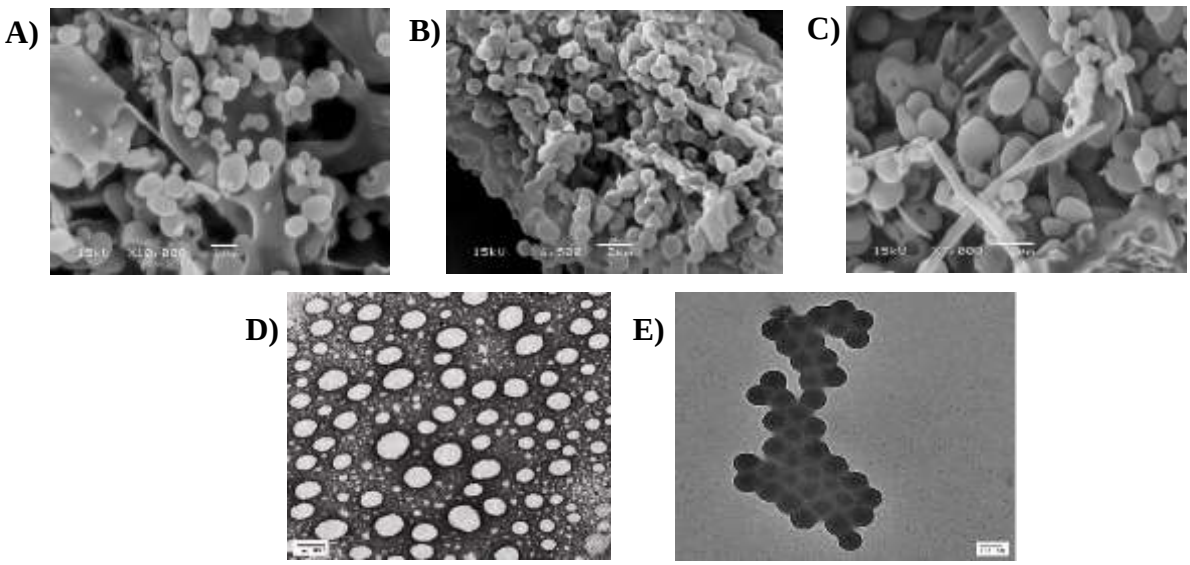

Figure 3. SEM micrograph of lyophilised nanoparticles: A) GG-OX4 (Bar: 1µm), B) PUL-OX4 (Bar: 2µm), C) CS-OX4 (Bar: 2µm), and TEM micrograph of nanoparticles from: D) PUL-OX4 (Bar: 100 nm, 2% uranyl acetate staining), and E) CS-OX4 (Bar: 100 nm, 2% uranyl acetate staining).

In order to monitor their fate *in vitro*, nanoparticles were fluorescently labelled using either Texas Red-X dichlorotriazine (for GG-OX4 and PUL-OX4) or Texas Red-X succinimidyl ester (for CS-OX4). The degree of labelling was determined as follows: 1.84% ± 0.51 for CS-OX4, 5.51% ± 1.29 for PUL-OX4, and 11.98% ± 2.56 for GG-OX4 (n=3, ±SD). CS-OX4 showed the lowest degree of labelling, likely due to the heterogeneous nature of the reaction (Sadki, 2011), which was carried out in suspension.

Model actives (MW 500-1000 Da, BCS class III or peptides (Benival & Devarajan, 2015; Volpe, 2004)) such as Doxorubicin and Rhodamine B that are known to be effluxed (Lee et al., 1994), and Angiotensin II were employed to investigate the drug loading and drug release profiles in/from the carriers. GG-OX4 nanoparticles exhibited the highest loading for Rhodamine B (3.78% ± 0.6) and Doxorubicin (19.11% ± 1.2), while Angiotensin II showed the highest load in PUL-OX4 (8.46% ± 1.0). Other results were presented as follows: CS-OX4 NPs had DL 1.38% ± 0.1, 3.56% ± 0.7, and 11.13% ± 1.6 for Rhodamine B, Angiotensin II and Doxorubicin respectively; GG-OX4 exhibited DL 6.11% ± 1.2 for Angiotensin II; and PUL-OX4 showed DL 2.11% ± 0.1 and 6.13% ± 0.8 for Rhodamine B and Doxorubicin respectively (n=3, ±SD). Overall, nanoparticles with negative zeta potential (GG-OX4 and PUL-OX4) demonstrated higher loading for positively-charged actives (Rhodamine B and Doxorubicin (Janes, Fresneau, Marazuela, Fabra, & Alonso, 2001; Selvam et al., 2008); Angiotensin II net charge +1.4) compared to CS-OX4 (with the only exception of Doxorubicin). The covalent cross-linking of GG-OX4 NPs with glutaraldehyde is likely to have contributed positively to their good loading degree performance (George, Shah, & Shrivastav, 2019) when compared to the other two modified polysaccharides.

A similar release profile was observed for all types of nanoparticles *(Figure 4)*, where an initial burst was followed by a plateau; this can be explained by the rapid release of the drug adsorbed on the surface (Fu & Kao, 2010; Ottenbrite & Kim, 2000) and the porous structure of the polymer matrix resulted from the lyophilisation. Interestingly, a delayed release of almost 1 h and a very slow release afterwards were observed in all cases for Doxorubicin, possibly because of a combined effect of a lower drug solubility in the saline employed as release medium and stronger drug interactions with the matrix (especially for cross-linked nanoparticles obtained from GG-OX4 and CS-OX4).

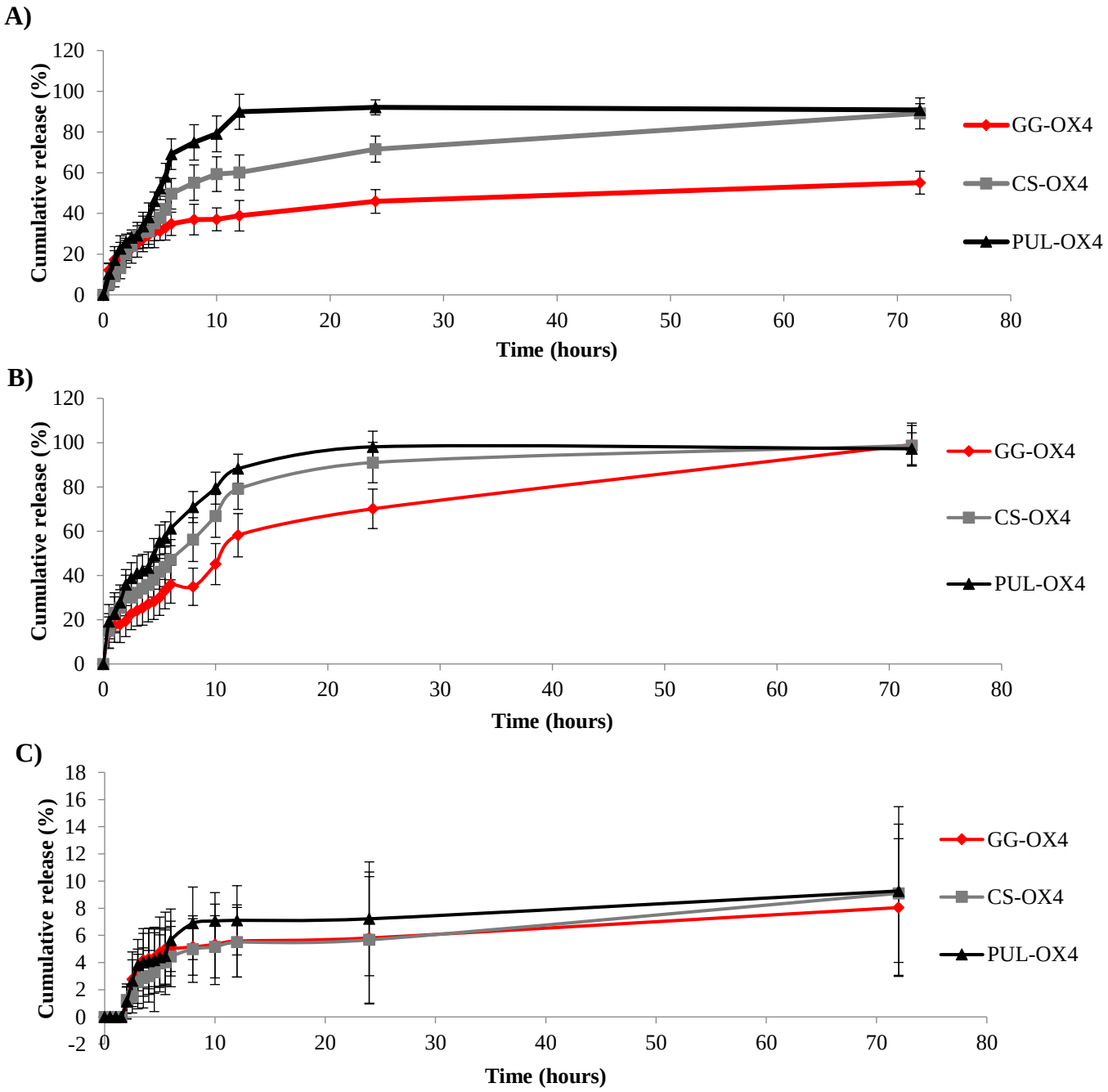

Figure 4. Release profiles of: A) Rhodamine B, B) Angiotensin II, C) Doxorubicin from loaded nanoparticles (1 mg/ml) in PBS (pH 7.4; saline 0.9%) (n=3, ±SD).

The obtained drug release data were fitted in Higuchi, Hixon-Crowell and Korsmeyer-Peppas kinetic models, and the quality of the fit was evaluated using the squared correlation coefficient (R^2). Doxorubicin release was found to be well described by the Korsmeyer-Peppas model, which indicated it is controlled by Fickian diffusion ($n < 0.5$), in contrast to the slow-release behaviour mentioned in literature for Doxorubicin loaded into chitosan-stearic acid

micelles (Xie, Du, Yuan, & Hu, 2012). Angiotensin II release from GG-OX4 and PUL-OX4 NPs can be well described by the Higuchi's model, and it was found to be controlled only by drug diffusion. For CS-OX4 NPs, the best fit was found with the Korsmeyer-Peppas model, which indicated the release was controlled by non-Fickian transport ($n > 0.5$), possibly through a combination of swelling and diffusion controlled release (Gulati, Nagaich, & Saraf, 2013). The Korsmeyer-Peppas model was the best fit for Rhodamine B release from GG-OX4 ($n < 0.5$; Fickian diffusion), CS-OX4 ($n > 0.5$; non-Fickian diffusion), and PUL-OX4 NPs ($n > 1$; super case II transport involving matrix swelling (Sahoo, Chakraborti, & Behera, 2012)).

An MTT assay was employed to study cytotoxicity of nanoparticles at different concentrations (1–10 mg/mL), using PBS and Triton-X (0.1% v/v) as controls. The results (*Figure 5)* showed that for application relevant concentrations (< 2 mg/mL) the cytotoxicity was not significant compared to the PBS control, where nanoparticles showed 85% cell viability. An increased cytotoxicity was observed however at higher concentrations (≥ 4 mg/mL), where the cell viability decreased below 75%, similar to the results reported for nanoparticles prepared from dextran modified with alkylglycidyl ether (Toman et al., 2015).

The LC_{50} (lethal concentration 50) on bEnd3 cells was determined, it was found that PUL-OX4 NPs exhibited the lowest toxicity (LC_{50} 9.48 ±0.98 mg/mL), followed by GG-OX4 (LC_{50} 8.84 ±0.76 mg/mL), with CS-OX4 showing the highest toxicity (LC_{50} 7.30 ±0.77 mg/mL).

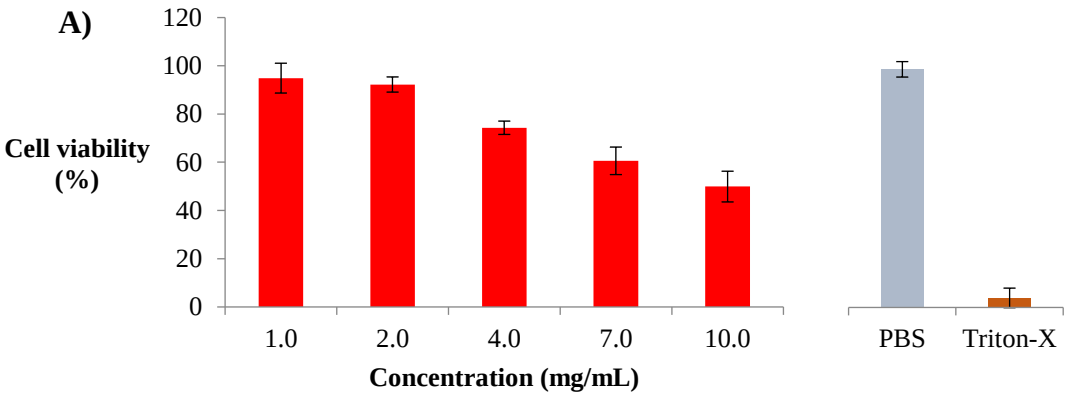

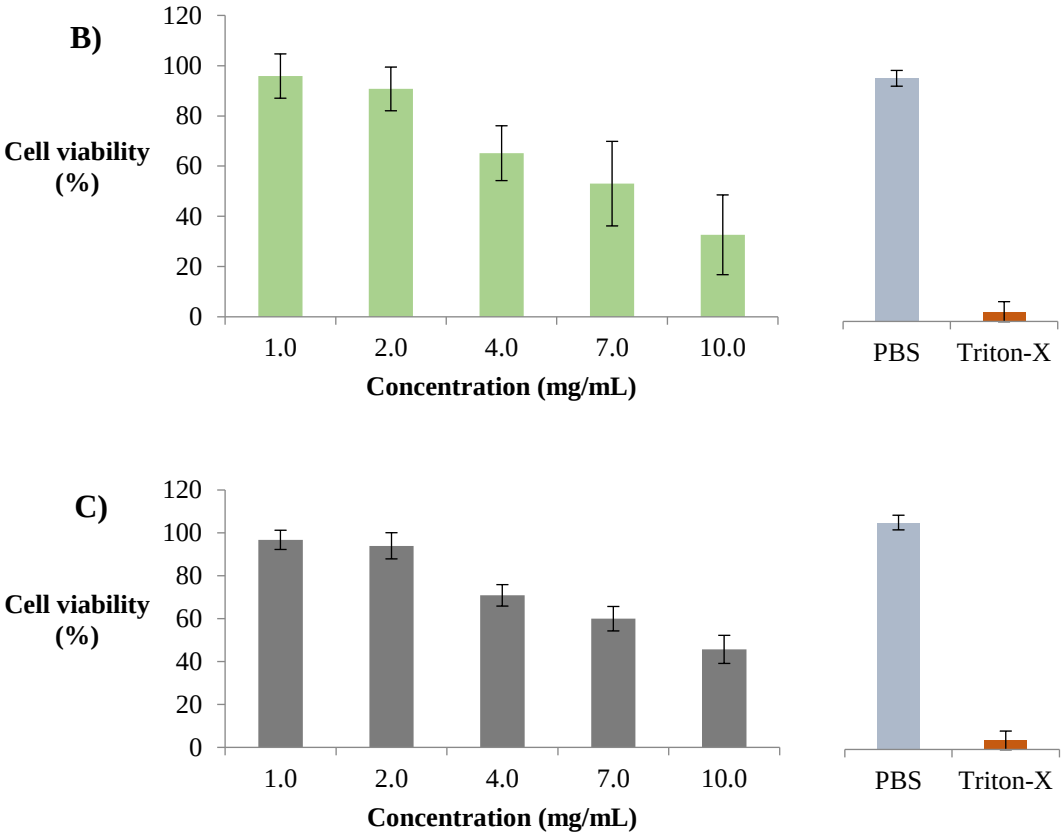

Figure 5. Nanoparticles relative cytotoxicity against bEnd3 cells: A) PUL-OX4, B) CS-OX4, and C) GG-OX4. bEnd3 cells incubated with nanoparticles (1–10 mg/mL); PBS and Triton-X (0.1% v/v) as controls (n=36, ±SD).

The interactions of nanoparticles with bEnd3 cells was investigated further using confocal microscopy and employing Texas Red-labelled nanoparticles (*Figure 6)*. Results suggest the NPs were taken up by cells and localised in the cytoplasm, appearing not to enter the nucleus), as previously found with butylglyceryl-modified chitosan nanoparticles (Lien et al., 2012); the uptake is suggested as being triggered *via* caveolar/clathrin-mediated endocytosis (Petros & DeSimone, 2010). Aggregation of nanoparticles outside cells and at the interface with the cell membranes was observed for CS-OX4, due to a lower stability of CS-OX4 formulations at pH 7.4 combined with the effect of the interactions between positively-charged nanoparticles and negatively-charged cell membrane.

Results obtained from flow cytometry recorded a higher than 85% uptake. PUL-OX4 nanoparticles (99.32%) exhibited the highest and CS-OX4 showed the lowest (87.88%; likely because of nanoparticles clustering, evidenced by the stability and confocal microscopy results), while GG-OX4 also exhibited a relatively high uptake with 95.25%.

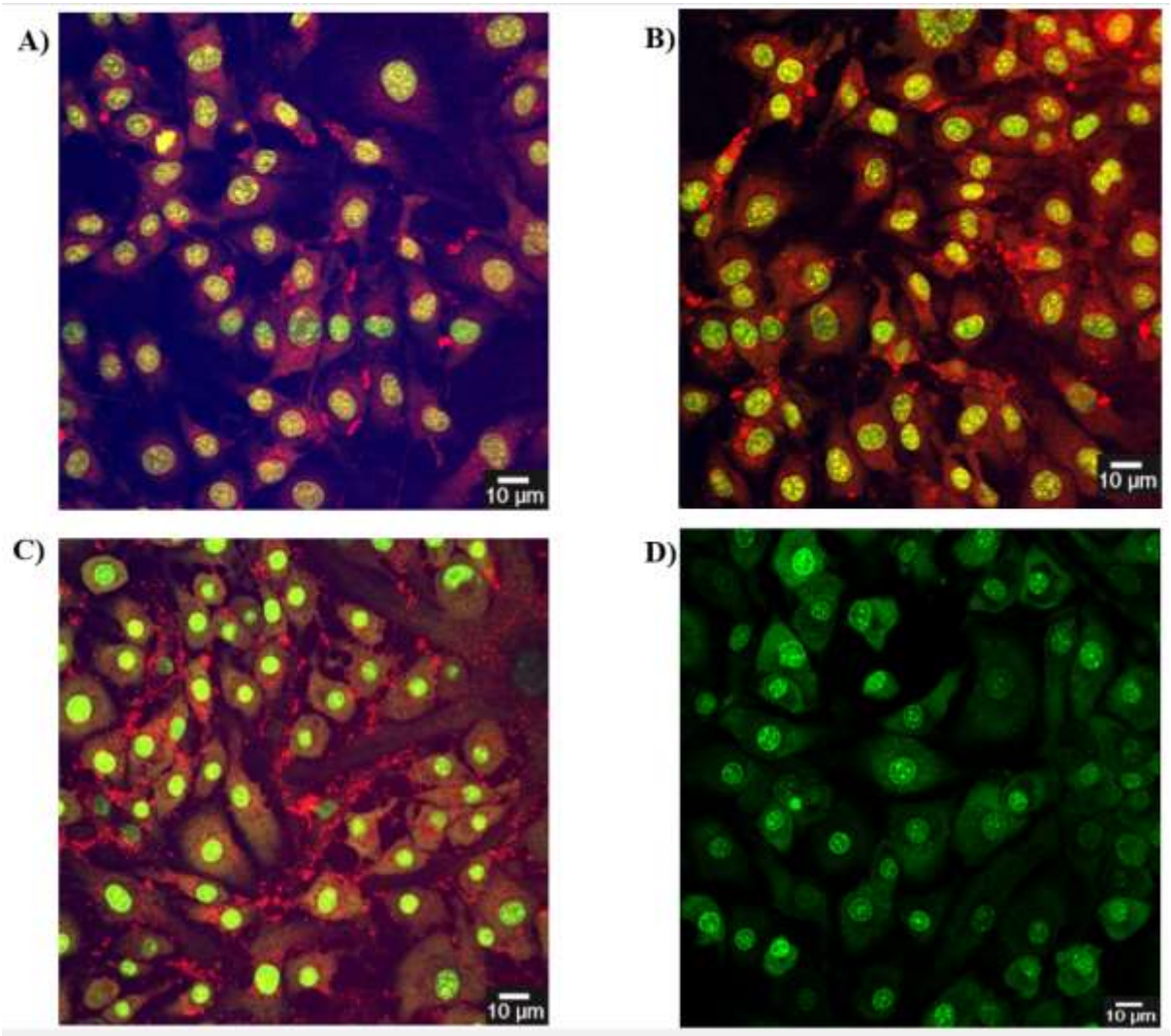

Figure 6. Confocal microscope images of bEnd3 cells treated with Texas Red-labelled nanoparticles (in red) from: A) PUL-OX4, B) GG-OX4, and C) CS-OX against black background. bEnd3 cells treated with NucGreen Dead 488 (in green; without nanoparticles) was used as a control (D) – Bar: 10 µm.

The effect on bEnd3 cells permeability was investigated using a Transwell-type BBB model comprising of a confluent bEnd3 cells monolayer enriched with a barrier enhancing formula (Lien et al., 2012); FITC-dextran (500 kDa) as a fluorescent marker. The longer the incubation time, the higher the permeability as noted for CS-OX4 and PUL-OX4 showing a significant effect after 3 h (*Figure 7)*, in contrast to GG-OX4.

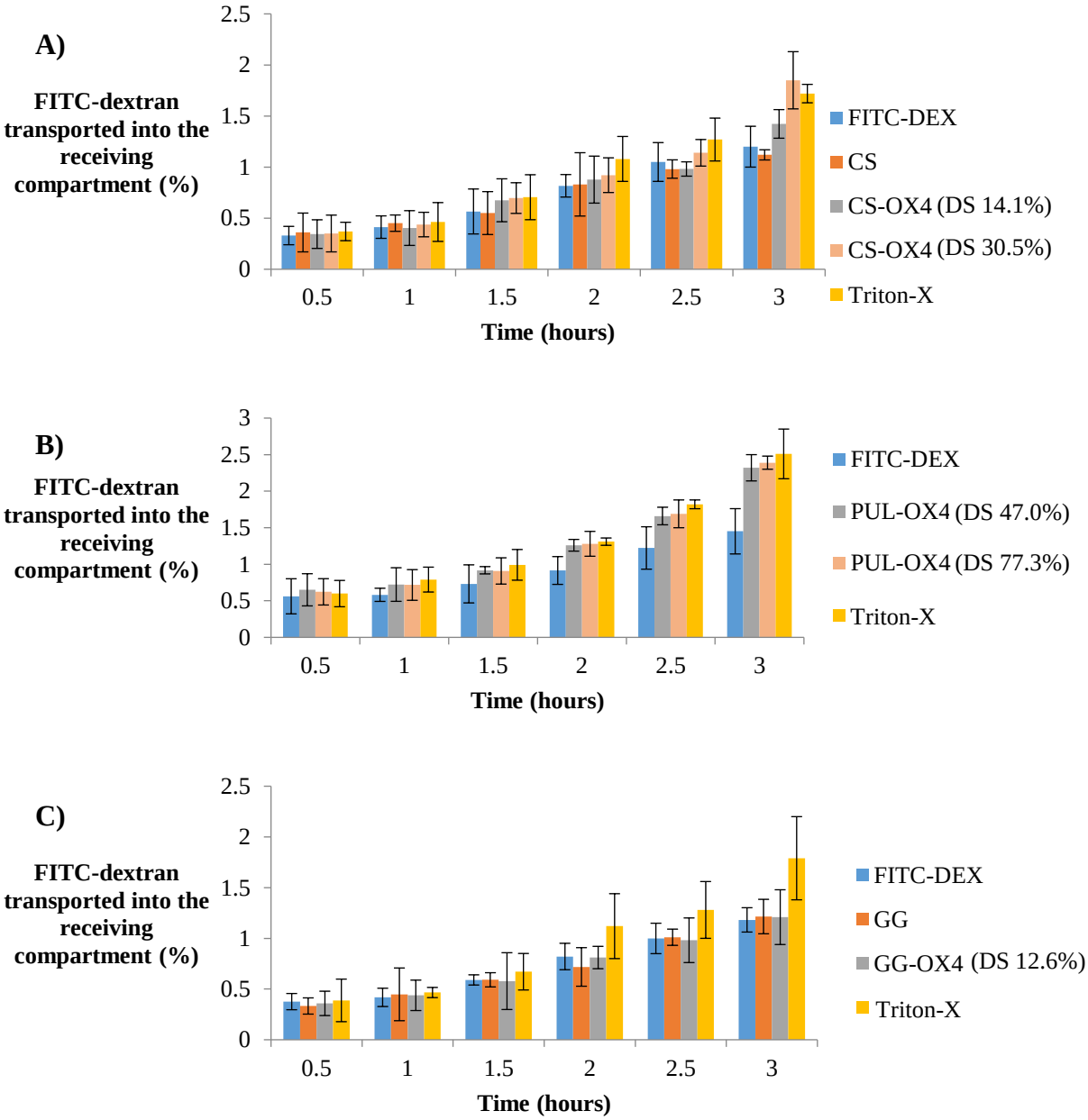

Figure 7. FITC-DEX translocation through bEnd3 cell monolayers following treatment with nanoparticles (2 mg/mL) prepared from either native polysaccharides or butylglyceryl-modified polysaccharide: A) CS-OX4, B) PUL-OX4, and C) GG-OX4. FITC-dextran and Triton-X (0.2 %) were employed as controls (n=5, ±SD).

The results of permeability studies (summarised in *Table 2)* indicated that the FITC-dextran paracellular transport across the bEnd3 monolayer increased with the DS; PUL-OX4 (DS 77.3%) showed the highest permeability enhancing effect (P_{app} value of 5.64 x 10^{-5} at 3 h); this value is higher than previously reported for alkylglyceryl-modified dextran with DS 130–142%; (1.5–1.6 x 10^{-7}; (Toman et al., 2015). No significant toxicity was induced at the concentration of 2 mg/mL, therefore it was assumed the translocation is not related to any

model membrane leaks associated with cell death. A concentration dependent effect was observed, however the trend was inconsistent for GG-OX4 (possibly because of the low DS of GG-OX4 used).

Table 2. Permeability coefficients (P_{app}) calculated from experiments using mouse bEnd3 cells treated with nanoparticles (2 mg/mL) at 3 h incubation time. FITC-DEX and Triton-X as controls (n=5, ±SD).

Material	Degree of substitution (%)	Concentration	P_{app} 3 hours
FITC-DEX	-	100 µg/mL	$(3.28 \pm 0.09) \times 10^{-5}$
CS	0	2.0 mg/mL	$(3.21 \pm 0.04) \times 10^{-5}$
CS-OX4	14.1	0.5 mg/mL	$(3.55 \pm 0.14) \times 10^{-5}$
	30.5	0.5 mg/mL	$(4.11 \pm 0.25) \times 10^{-5}$
		2.0 mg/mL	$(4.94 \pm 0.28) \times 10^{-5}$
PUL-OX4	47.0	2.0 mg/mL	$(4.55 \pm 0.19) \times 10^{-5}$
	77.3	0.5 mg/mL	$(4.64 \pm 0.13) \times 10^{-5}$
		2.0 mg/mL	$(5.64 \pm 0.09) \times 10^{-5}$
GG	0	2.0 mg/mL	$(3.38 \pm 0.20) \times 10^{-5}$
GG-OX4	12.6	0.5 mg/mL	$(3.36 \pm 0.23) \times 10^{-5}$
		2.0 mg/mL	$(3.56 \pm 0.18) \times 10^{-5}$
Triton-X	-	0.2 % v/v	$(6.97 \pm 0.33) \times 10^{-5}$

Rationalised by the fact that most of the therapeutic applications are intravenous-based, a haemolysis study was performed in order to investigate the potential toxicity of nanoparticles towards red blood cells, RBC (*Figure 8)*; the NP concentration effect on the RBC lysis was also studied. Results indicated no toxicity at concentrations below 12 mg/mL, showing less than 10% haemolysis compared to the PBS control. A certain degree of haemolysis was found however with increasing the concentration further, and calculated LC_{30} values (19.87 mg/mL, 18.01 mg/mL, and 13.95 mg/mL for PUL-OX4, GG-OX4, and CS-OX4, respectively) indicated that PUL-based NPs exhibit the least haemolytic effect. In contrast, at high concentrations, CS-OX4 nanoparticles were found to induce the strongest haemolytic effect, likely due to interactions between positively-charged chitosan and negatively-charged cell membranes leading to membrane damage (Narayanan, Anitha, Jayakumar, Nair, & Chennazhi, 2012).

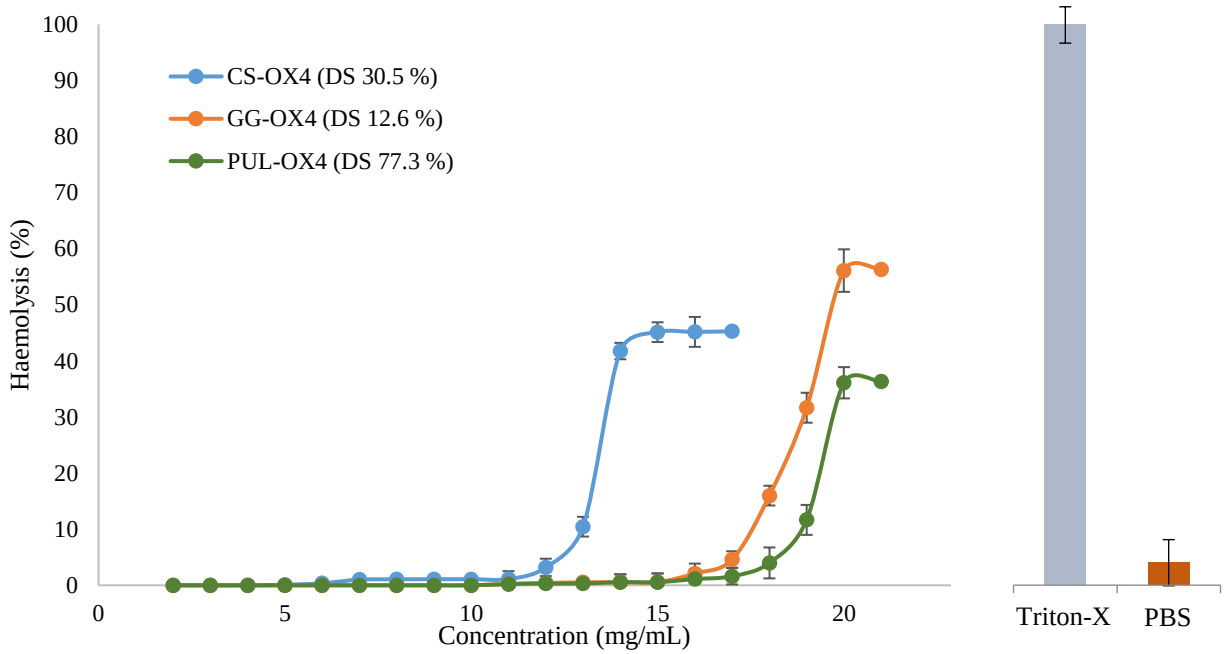

Figure 8. Haemolysis test results using rat RBC exposed to butylglyceryl-modified nanoparticles of varying concentrations. RBC suspension mixed with PBS or Triton-X (1%) were used as controls (n=3; ±SD).

4. Conclusions

Amphiphilic butylglyceryl derivatives of guar gum, pullulan, and chitosan (prepared *via* modification with *n*-butylglycidyl ether) can be formulated using various methods into nanogels (120–200 nm diameter) to be employed as drug carriers. However, only PUL-OX4 colloidal formulations demonstrated acceptable stability over the whole range of pH tested (3 - 8.5).

GG-OX4 NPs showed the highest loading capacity for high molecular weight model actives that are known to be effluxed (such as Rhodamine B and Doxorubicin), while PUL-OX4 NPs were found to perform better for high molecular weight and hydrophilic biomacromolecules such as Angiotensin II peptide; the drug release profiles can be best described by either Korsmeyer-Peppas or Higuchi equations, and showed in all cases an initial burst discharge followed by a gradual release phase.

PUL-OX4 NPs demonstrated the lowest cytotoxicity (i.e. highest LC_{50} value, as determined by MTT) and the weakest haemolytic effect. All NPs were taken up by bEnd3 brain endothelial cells, with PUL-OX4 NPs showing the highest uptake. The presence of butylglyceryl-modified nanoparticles enhanced the FITC-DEX transport across the bEnd3-

based BBB model membranes, with PUL-OX4 nanoparticles showing the highest drug permeability enhancing effect. Overall, our results suggest that PUL-OX4 nanoparticles would warrant further development as they demonstrate most promising characteristics for potential use in brain drug delivery applications.

Acknowledgements

This study was supported by the Majlis Amanah Rakyat (Malaysia), University of Portsmouth (UK), and Al Ain University (UAE).

References

Barbosa, J. A. C., Abdelsadig, M. S. E., Conway, B. R., & Merchant, H. A. (2019). Using zeta potential to study the ionisation behaviour of polymers employed in modified-release dosage forms and estimating their pKa. *International journal of pharmaceutics: X, 1*, 100024.

Benival, D. M., & Devarajan, P. V. (2015). In situ lipidization as a new approach for the design of a self microemulsifying drug delivery system (SMEDDS) of doxorubicin hydrochloride for oral administration. *Journal of biomedical nanotechnology, 11*(5), 913-922.

Bostanudin, M. F., Arafat, M., Sarfraz, M., Górecki, D. C., & Barbu, E. (2019). Butylglyceryl pectin nanoparticles: synthesis, formulation and characterization. *Polymers, 11*(5), 789.

Boussahel, A., Ibegbu, D. M., Lamtahri, R., Maucotel, J., Chuquet, J., Lefranc, B., . . . Gorecki, D. (2017). Investigations of octylglyceryl dextran-graft-poly (lactic acid) nanoparticles for peptide delivery to the brain. *Nanomedicine, 12*(8), 879-892.

Chen, Y., Mohanraj, V. J., Wang, F., & Benson, H. A. E. (2007). Designing chitosan-dextran sulfate nanoparticles using charge ratios. *AAPS PharmSciTech, 8*(4), 131-139.

Erdlenbruch, B., Schinkhof, C., Kugler, W., Heinemann, D. E. H., Herms, J., Eibl, H., & Lakomek, M. (2003). Intracarotid administration of short-chain alkylglycerols for increased delivery of methotrexate to the rat brain. *British journal of pharmacology, 139*(4), 685-694.

Fu, Y., & Kao, W. J. (2010). Drug release kinetics and transport mechanisms of non-degradable and degradable polymeric delivery systems. *Expert opinion on drug delivery, 7*(4), 429-444.

George, A., Shah, P. A., & Shrivastav, P. S. (2019). Guar gum: Versatile natural polymer for drug delivery applications. *European Polymer Journal, 112*, 722-735.

Godfrey, L., Iannitelli, A., Garrett, N. L., Moger, J., Imbert, I., King, T., . . . Schätzlein, A. G. (2018). Nanoparticulate peptide delivery exclusively to the brain produces tolerance free analgesia. *Journal of controlled release, 270*, 135-144.

Gulati, N., Nagaich, U., & Saraf, S. A. (2013). Intranasal delivery of chitosan nanoparticles for migraine therapy. *Scientia pharmaceutica, 81*(3), 843.

Hervé, F., Ghinea, N., & Scherrmann, J.-M. (2008). CNS delivery via adsorptive transcytosis. *The AAPS journal, 10*(3), 455-472.

Hongbo, T., Yanping, L., Wen, Z., & Siqing, D. (2016). Synthesis, optimization, property, characterization, and application of dialdehyde cross-linking guar gum. *International Journal of Polymer Science, 2016*.

Ibegbu, D. M., Boussahel, A., Cragg, S. M., Tsibouklis, J., & Barbu, E. (2017). Nanoparticles of alkylglyceryl dextran and poly (ethyl cyanoacrylate) for applications in drug delivery: Preparation and characterization. *International Journal of Polymeric Materials and Polymeric Biomaterials, 66*(6), 265-279.

Janes, K. A., Fresneau, M. P., Marazuela, A., Fabra, A., & Alonso, M. a. J. (2001). Chitosan nanoparticles as delivery systems for doxorubicin. *Journal of controlled Release, 73*(2-3), 255-267.

Jung, S.-W., Jeong, Y.-I., Kim, Y.-H., & Kim, S.-H. (2004). Self-assembled polymeric nanoparticles of poly (ethylene glycol) grafted pullulan acetate as a novel drug carrier. *Archives of pharmacal research, 27*(5), 562-569.

Lalatsa, A., & Barbu, E. (2016). Carbohydrate nanoparticles for brain delivery. In *International review of neurobiology* (Vol. 130, pp. 115-153): Elsevier.

Lalatsa, A., Schatzlein, A. G., & Uchegbu, I. F. (2014). Strategies to deliver peptide drugs to the brain. *Molecular pharmaceutics, 11*(4), 1081-1093.

Lalatsa, A., Schätzlein, A. G., Garrett, N. L., Moger, J., Briggs, M., Godfrey, L., . . . Uchegbu, I. F. (2015). Chitosan amphiphile coating of peptide nanofibres reduces liver uptake and delivers the peptide to the brain on intravenous administration. *Journal of Controlled Release, 197*, 87-96.

Lee, J.-S., Paull, K., Alvarez, M., Hose, C., Monks, A., Grever, M., . . . Bates, S. E. (1994). Rhodamine efflux patterns predict P-glycoprotein substrates in the National Cancer Institute drug screen. *Molecular pharmacology, 46*(4), 627-638.

Lien, C.-F., Molnár, E. v., Toman, P., Tsibouklis, J., Pilkington, G. J., Górecki, D. C., & Barbu, E. (2012). In vitro assessment of alkylglyceryl-functionalized chitosan nanoparticles as permeating vectors for the blood–brain barrier. *Biomacromolecules, 13*(4), 1067-1073.

Lu, C.-T., Zhao, Y.-Z., Wong, H. L., Cai, J., Peng, L., & Tian, X.-Q. (2014). Current approaches to enhance CNS delivery of drugs across the brain barriers. *International journal of nanomedicine, 9*, 2241.

Molnár, E. v., Barbu, E., Lien, C.-F., Górecki, D. C., & Tsibouklis, J. (2010). Toward drug delivery into the brain: synthesis, characterization, and preliminary in vitro assessment of alkylglyceryl-functionalized chitosan nanoparticles. *Biomacromolecules, 11*(11), 2880-2889.

Narayanan, D., Anitha, A., Jayakumar, R., Nair, S. V., & Chennazhi, K. P. (2012). Synthesis, characterization and preliminary in vitro evaluation of PTH 1-34 loaded chitosan nanoparticles for osteoporosis. *Journal of biomedical nanotechnology, 8*(1), 98-106.

Ottenbrite, R. M., & Kim, S. W. (2000). *Polymeric drugs and drug delivery systems*: CRC Press.

Pal, K., Paulson, A. T., & Rousseau, D. (2009). Biopolymers in controlled-release delivery systems. In *Modern biopolymer science* (pp. 519-557): Elsevier.

Petros, R. A., & DeSimone, J. M. (2010). Strategies in the design of nanoparticles for therapeutic applications. *Nature reviews Drug discovery, 9*(8), 615-627.

Raggi, A., & Leonardi, M. (2019). Burden of brain disorders in Europe in 2017 and comparison with other non-communicable disease groups. *Journal of Neurology, Neurosurgery & Psychiatry*, jnnp-2019.

Sadki, M. S. (2011). Hydrophobically modified derivatives of polysaccharides.

Sahoo, S., Chakraborti, C. K., & Behera, P. K. (2012). Development and evaluation of gastroretentive controlled release polymeric suspensions containing ciprofloxacin and carbopol polymers. *J Chem Pharm Res, 4*, 2268-2284.

Selvam, P. P., Preethi, S., Basakaralingam, P., Thinakaran, N., Sivasamy, A., & Sivanesan, S. (2008). Removal of rhodamine B from aqueous solution by adsorption onto sodium montmorillonite. *Journal of Hazardous Materials, 155*(1-2), 39-44.

Singh, R. S., Kaur, N., Rana, V., & Kennedy, J. F. (2017). Pullulan: a novel molecule for biomedical applications. *Carbohydrate polymers, 171*, 102-121.

Toman, P., Lien, C.-F., Ahmad, Z., Dietrich, S., Smith, J. R., An, Q., . . . Tsibouklis, J. (2015). Nanoparticles of alkylglyceryl-dextran-graft-poly (lactic acid) for drug delivery to the brain: Preparation and in vitro investigation. *Acta biomaterialia, 23*, 250-262.

Volpe, D. A. (2004). Permeability classification of representative fluoroquinolones by a cell culture method. *AAPS PharmSci, 6*(2), 1-6.

Wang, Q. Z., Chen, X. G., Liu, N., Wang, S. X., Liu, C. S., Meng, X. H., & Liu, C. G. (2006). Protonation constants of chitosan with different molecular weight and degree of deacetylation. *Carbohydrate polymers, 65*(2), 194-201.

Xie, Y.-T., Du, Y.-Z., Yuan, H., & Hu, F.-Q. (2012). Brain-targeting study of stearic acid–grafted chitosan micelle drug-delivery system. *International journal of nanomedicine, 7*, 3235.